Article

Discovery Medicine 2024; 36(183): 730–738
https://doi.org/10.24976/Discov.Med.202436183.69

Visual Interpretation of Radiomics Features in Filtered Computed Tomography Images during the Portal Phase of Acute Pancreatitis

Wenjing He[1,†], Mingyue Tang[2,†], Xian Jiang[1], Bo Xiao[3], Jiayi Wei[1], Yanmei Zhao[1], Yuanzhong Zhu[1], Xiaowen Chen[1,*]

[1]School of Medical Imaging, North Sichuan Medical College, 637000 Nanchong, Sichuan, China
[2]School of Basic Medicine and Forensic Medicine, North Sichuan Medical College, 637000 Nanchong, Sichuan, China
[3]Department of Radiology, Bishan Hospital of Chongqing Medical University, 402760 Chongqing, China
*Correspondence: 56833804@qq.com (Xiaowen Chen)
[†]These authors contributed equally.
Published: 20 April 2024

Background: Current research on radiomics for diagnosing and prognosing acute pancreatitis predominantly revolves around model development and testing. However, there is a notable absence of ongoing interpretation and analysis regarding the physical significance of these models and features. Additionally, there is a lack of extensive exploration of visual information within the images. This limitation hinders the broad applicability of radiomics findings. This study aims to address this gap by specifically analyzing filtered Computed Tomography (CT) image features of acute pancreatitis to identify meaningful visual markers in the pancreas and peripancreatic area.

Methods: Numerous filtered CT images were obtained through pyradiomics. The window width and window level were fine-tuned to emphasize the pancreas and peripancreatic regions. Subsequently, the LightGBM algorithm was employed to conduct an embedded feature screening, followed by statistical analysis to identify features with statistical significance (p-value < 0.01). Within the purview of the study, for each filtering method, features of high importance to the preceding prediction model were incorporated into the analysis. The image visual markers were then systematically sought in reverse, and their medical interpretation was undertaken to a certain extent.

Results: In Laplacian of Gaussian filtered images within the pancreatic region, severe acute pancreatitis (SAP) exhibited fewer small areas with repetitive greyscale patterns. Conversely, in the peripancreatic region, SAP displayed greater irregularity in both area size and the distribution of greyscale levels. In logarithmic images, SAP demonstrated reduced low greyscale connectivity in the pancreatic region, while showcasing a higher average variation in greyscale between two adjacent pixels in the peripancreatic region. Moreover, in gradient images, SAP presented with decreased repetition of two adjacent pixel greyscales within the pancreatic region, juxtaposed with an increased inhomogeneity in the size of the same greyscale region within the δ range in the peripancreatic region.

Conclusions: Various filtered images convey distinct physical significance and properties. The selection of the appropriate filtered image, contingent upon the characteristics of the Region of Interest (ROI), enables a more comprehensive capture of the heterogeneity of the disease.

Keywords: acute pancreatitis; Laplacian of Gaussian filters; logarithmic filters; gradient filters

Introduction

Acute pancreatitis (AP) stands out as one of the most prevalent forms of acute abdominal pain. The majority of AP cases are characterized as mild and self-limiting, typically resolving within a week. However, around 20% of individuals with AP progress to severe acute pancreatitis (SAP), which carries a significantly worse prognosis and an elevated mortality rate [1]. Consequently, the timely and accurate identification of AP severity is imperative to enhance patient prognosis and diminish mortality.

Most existing studies employing radiomics for disease diagnosis and prediction are primarily focused on modeling and testing. Unfortunately, these studies often fall short in providing continued interpretation and analysis of the physical meaning inherent in models and features. Moreover, they neglect the conduct of reverse searches for information within filtered visual images. Additionally, there is a lack of interpretation regarding filtered images and features, as well as a deficiency in further extracting visual information from images.

This limitation results in a dependency on software for the implementation of radiomics findings, making it challenging for clinicians to effectively leverage the analytical insights derived from radiomics models. Consequently, this hinders the widespread application of research results in clinical settings.

A model for early prediction of acute pancreatitis severity, based on Computed Tomography (CT) radiomics analyzing pancreatic and peripancreatic alterations, was developed in a prior study [2]. In this paper, we extend our investigation beyond the previous screening and modeling of radiomics features of AP to delve into the visual characteristics of the images post-application of Laplacian of Gaussian (LoG), logarithmic, exponential, square, and gradient filters [3–5].

Specifically, our focus lies in exploring the medical interpretation of image visuals associated with features from AP radiomics models. We aim to establish a connection between quantitative radiomics feature values and image visual markers. Our study offers a method to search for statistically significant biomarkers in various filtered images through radiomics feature screening and modeling. This approach enhances our understanding of the dataset, providing clinicians with means to conduct a preliminary analysis of the disease condition using filtered images.

Methods

Patients

The study involved a retrospective analysis of 215 patients experiencing their first-episode of AP. All subjects were admitted to the Affiliated Hospital of North Sichuan Medical College between January 1, 2016, and June 30, 2022. They were subsequently categorized into two groups: the non-severe acute pancreatitis (NSAP) group and the SAP group.

This retrospective study received approval from the ethics committee of North Sichuan Medical College (No. NSMC lunzhiwenshen[2023030]), and patients were exempted from providing informed consent. Inclusion criteria comprised individuals who: (1) met the diagnostic criteria of AP referring to the 2012 revised Atlanta Classification [6]; (2) were admitted for the first time; (3) underwent contrast enhanced-CT examination within 2 days of onset.

Exclusion criteria encompassed those with: (1) incomplete electronic medical records, including past and current medical history; (2) transfers from other medical facilities; (3) a history of cirrhosis or malignancy; (4) undergone major pelvic and abdominal surgery within the past month; (5) systemic infectious diseases; (6) poor-quality enhanced CT images.

Preliminary Model

Portal venous phase contrast-enhanced CT images in DICOM format were obtained from the picture archiving and communication system (PACS) for each patient. Two experienced radiologists, blinded to the diagnosis, outlined two Regions of Interest (ROI) using 3D slicer software version 4.2.2 (CIBC, Bethesda, MD, USA). The first ROI (label1) encompassed the entire pancreas, including necrotic areas while excluding blood vessels and bile ducts. The second ROI (label2) covered a large area of peripancreatic exudate and effusion (Fig. 1).

Utilizing PyRadiomics version 3.0.1 in Python (version 3.9.6), features were automatically extracted from each ROI, resulting in 1520 features for each label and a cumulative total of 3040 features. Subsequently, a radiomics logistic regression model was constructed following feature selection by LightGBM. The area under the curve (AUC) of this radiomics model was found to be 0.992 [95% confidence interval (CI): 0.963–0.996] in the training set, 0.965 (95% CI: 0.924–0.981) in the validation set, and 0.894 (95% CI: 0.789–0.966) in the test set.

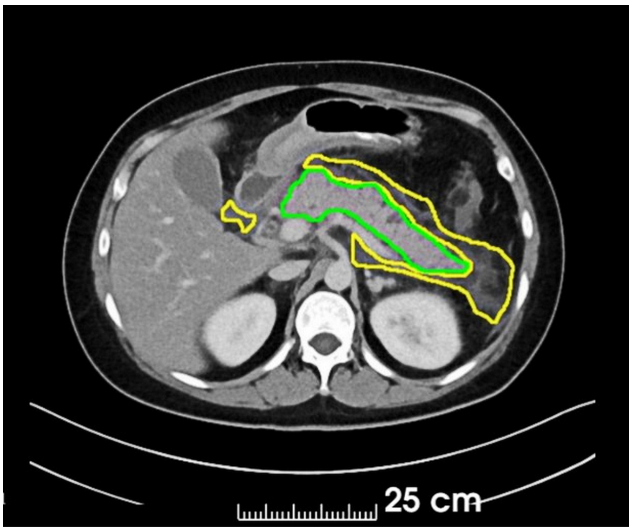

Fig. 1. Outlining of the Regions of Interest (ROI) Portal in venous phase contrast-enhanced Computed Tomography (CT) image. Green indicates label1, Yellow indicates label2.

Filtered Images and Image Biomarkers

In this study, we initially applied the LoG filter, logarithmic filter, gradient filter, exponential filter, and square filter to the original images using pyradiomics, resulting in filtered abdominal images. Subsequently, the window width and window level were adjusted to accentuate the two ROIs encompassing the pancreas and peripancreatic regions. The LightGBM algorithm was then employed to conduct embedded feature screening on the initial 3040 features. This was followed by an independent *t*-test analysis to identify features with statistical significance ($p < 0.01$). For each filter method under investigation, features of notable importance to the preceding prediction model were integrated into the analysis.

Table 1. Filter equations.

Filter name	Formula*	Interpretation
LoG Filter	$G(x,y,z,\sigma) = \frac{1}{\left(\sigma\sqrt{2\pi}\right)^3} e^{-\frac{x^2+y^2+z^2}{2\sigma^2}}$ $LoG = \nabla^2 G(x,y,z)$	$G = \frac{1}{16}\begin{bmatrix}1 & 2 & 1\\ 2 & 4 & 2\\ 1 & 2 & 1\end{bmatrix}$ $L = \begin{bmatrix}0 & -1 & 0\\ -1 & 4 & -1\\ 0 & -1 & 0\end{bmatrix}$
Logarithmic Filter	$f(x) = \begin{cases} c\log(x+1), x \geq 0 \\ -c\log(-x+1), x < 0 \end{cases}$, $c = \frac{max(\lvert x \rvert)}{\log(max(\lvert x \rvert)+1)}$	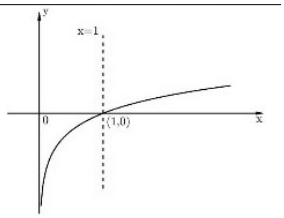
Gradient Filter	$\frac{\partial f(x,y)}{\partial x} \approx \frac{f(x+1,y) - f(x-1,y)}{2}$	$[-1 \quad 0 \quad 1]$
Exponential Filter	$f(x) = e^{cx}$, $c = \frac{\log(\max(\lvert x \rvert))}{\max(\lvert x \rvert)}$	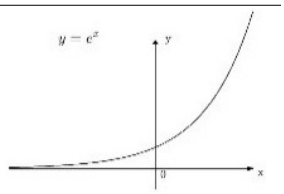
Square Filter	$f(x) = (cx)^2$, $c = \frac{1}{\sqrt{max(\lvert x \rvert)}}$	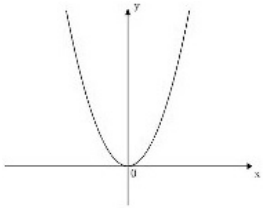

Footnote: G, Gaussian kernel; LoG, Laplacian of Gaussian.

*Formula source:

https://pyradiomics.readthedocs.io/en/latest/radiomics.html#radiomics.imageoperations.

The principle and applicability of each filtered image were scrutinized based on the corresponding formula (Table 1). Furthermore, an investigation into the physical meaning of the Gray Level Co-occurrence Matrix (GLCM), Gray Level Run Length Matrix (GLRLM), Gray Level Size Zone Matrix (GLSZM), Gray Level Dependence Matrix (GLDM) [7], and the respective feature formulae was undertaken. Lastly, image visual markers were systematically sought in reverse, and to some extent, medically interpreted.

Results

Demographic and Clinical Characteristics

This study enrolled a total of 215 patients with AP. The training cohort comprised 141 patients, consisting of 113 non-severe and 28 severe cases. In the test cohort, there were 74 patients, with 45 classified as non-severe and 29 as severe cases. The clinical information of the patients is detailed in Table 2.

Representative Features

Following feature screening and independent *t*-test analysis, a set of 68 features exhibiting significant correlations was identified. From this pool, a total of 6 representative features were meticulously chosen, each corresponding to different filtering methods (Table 3). For additional details regarding these representative features, readers are directed to the Image Biomarker Standardisation Initiative [8].

Laplacian of Gaussian (LoG) Filter

The LoG filter formula, along with the commonly used 2-dimensional filter templates, is presented in Table 1. G (x, y, z, σ) represents a 3D Gaussian filtering factor implemented through a discretized convolutional sliding window. The template G is a 3 $\times$ 3 Gaussian filter, forming a low-pass filter with smoothing properties. This filter computes the value of each pixel point as a weighted average of itself and the pixel values within a range of σ. Utilizing G contributes to noise reduction in the image.

The LoG filter is used for two steps: it first applies a Gaussian filter to the image and then performs a Laplacian filter. This approach enhances portions of the image with significant local grey level variations [9]. The size of the sliding window is determined by σ, and a larger σ re-

Table 2. Characteristics of the patients in the training and test cohorts.

Characteristics	Training cohort (n = 141)				Test cohort (n = 74)			
	Nonsevere AP (n = 113)	Severe AP (n = 28)	Statistical value	*p* value	Nonsevere AP (n = 45)	Severe AP (n = 29)	Statistical value	*p* value
Age (years)	49.8 ± 15.4	57.6 ± 17.0	t = –2.34	0.021	55.1 ± 18.7	56.0 ± 16.6	t = –0.21	0.834
Sex (male)	71 (62.83%)	16 (57.17%)	$\chi^2 = 0.31$	0.579	26 (57.78%)	15 (51.72%)	$\chi^2 = 0.26$	0.609
Etiology, n (%)			$\chi^2 = 1.30$	0.521			$\chi^2 = 7.65$	0.022
Biliary	26 (23.01%)	8 (28.57%)			18 (40.00%)	14 (48.28%)		
Hyperlipemia	41 (36.28%)	7 (25.00%)			8 (17.78%)	11 (37.39%)		
Others	46 (40.71%)	13 (46.43%)			19 (42.22%)	4 (13.79%)		
Type of AP			$\chi^2 = 10.73$	<0.001			$\chi^2 = 25.5$	<0.001
Acute edematous pancreatitis	101 (89.38%)	18 (64.29%)			44 (97.78%)	14 (48.28%)		
Acute necrotizing pancreatitis	12 (10.62%)	10 (35.71%)			1 (2.22%)	15 (51.72%)		

AP, acute pancreatitis.

Table 3. Representative features of AP classification.

Feature		NSAP	SAP	*t*-value	*p*-value
1	label1-log-sigma-4-0-mm-3D_gldm_SmallDependenceEmphasis	0.02700 ± 0.00952	0.02070 ± 0.00838	3.160	<0.001
2	label1-logarithm_glszm_LowGrayLevelZoneEmphasis	0.00759 ± 0.00425	0.00457 ± 0.00179	5.715	<0.001
3	label1-gradient_glcm_JointEntropy	0.46400 ± 0.33600	0.23300 ± 0.29100	3.576	<0.001
4	label2-log-sigma-2-0-mm-3D_glszm_ZoneEntropy	3.87000 ± 0.86500	4.58000 ± 0.4500	–5.962	<0.001
5	label2-logarithm_glcm_DifferenceAverage	9.51000 ± 6.29000	17.8000 ± 8.35000	–4.836	<0.001
6	label2-gradient_gldm_DependenceVariance	26.70000 ± 13.70000	36.90000 ± 6.06000	–5.873	<0.001

SAP, severe acute pancreatitis; NSAP, non-severe acute pancreatitis.

sults in a larger window and a wider range of adjacent pixel values influencing the center's determination. A smaller σ value in the LoG filter emphasizes grey level changes in the ROI at a closer distance to the observed pixels, revealing finer details. Conversely, a larger σ value highlights grey level changes at a greater distance, providing a more holistic view of the ROI. The LoG filter effectively reduces Gaussian noise and simultaneously enhances grey-scale abrupt sections of the image.

As illustrated in Fig. 2, a LoG-filtered image with different σ values showcases enhanced contours of tissue and organ structures, attributing to robust grey-scale variations.

In Table 3, features 1 and 4 were identified as representative features after LoG filtering. The physical interpretation of feature 1 involves the ROI of the pancreatic region (label1), where the central pixel was considered at $\sigma = 4$. This implies that the value of the filtered central pixel was determined by the 81 pixels within a distance of 0–4 from the central pixel. Specifically, "gldm_SmallDependenceEmphasis" signifies that the image GLDM was generated, and its SmallDependenceEmphasis value was computed. In the GLDM, each row represents a grey level, columns denote the size of the area where the grey recurs within the range δ, and the matrix elements indicate the number of occurrences for that grey level and size. The SmallDependenceEmphasis feature value, derived from the GLDM, tends to be larger when there are more small regions with repeated grey levels in the δ range.

As depicted in Fig. 2, panels C and F showcase LoG-filtered images at $\sigma = 4$ for one case of NSAP and one case of SAP, respectively. In this dataset, the mean value for NSAP was 0.027, whereas for SAP, it was 0.0207 ($p < 0.001$), signifying statistical significance. This suggests that SAP tends to exhibit a lower value for this feature, indicating a more segmented area formed by different grey levels within the ROI in the images. Visually, it is observed that the same shades of grey within the ROI of the pancreas in Fig. 2F are more likely to be contiguous than those in Fig. 2C.

Feature 4 pertains to the central pixel neighborhood within the peripancreatic area (label2) ROI, considering $\sigma = 2$. This signifies that the value of the filtered central pixel was determined by the 25 pixels within a distance of 0–2 from the central pixel. Specifically, "glszm ZoneEntropy" denotes that the ZoneEntropy was computed after obtaining the Grey Level Size Zone Matrix (GLSZM) of the image. In the GLSZM, different rows represent various grey levels, columns indicate the sizes of connected areas, and matrix elements depict the number of occurrences of the same grey connected area. The ZoneEntropy metric measures the randomness of the ROI region size and the distribution of grey levels. Higher values indicate more irregularity and uncertainty in the area size of the same grey level sub-region.

According to feature 4, the mean value for NSAP in this dataset was 3.87, while the mean for SAP was 4.58, a statistically significant difference ($p < 0.001$). This suggests that as the severity of acute pancreatitis increases,

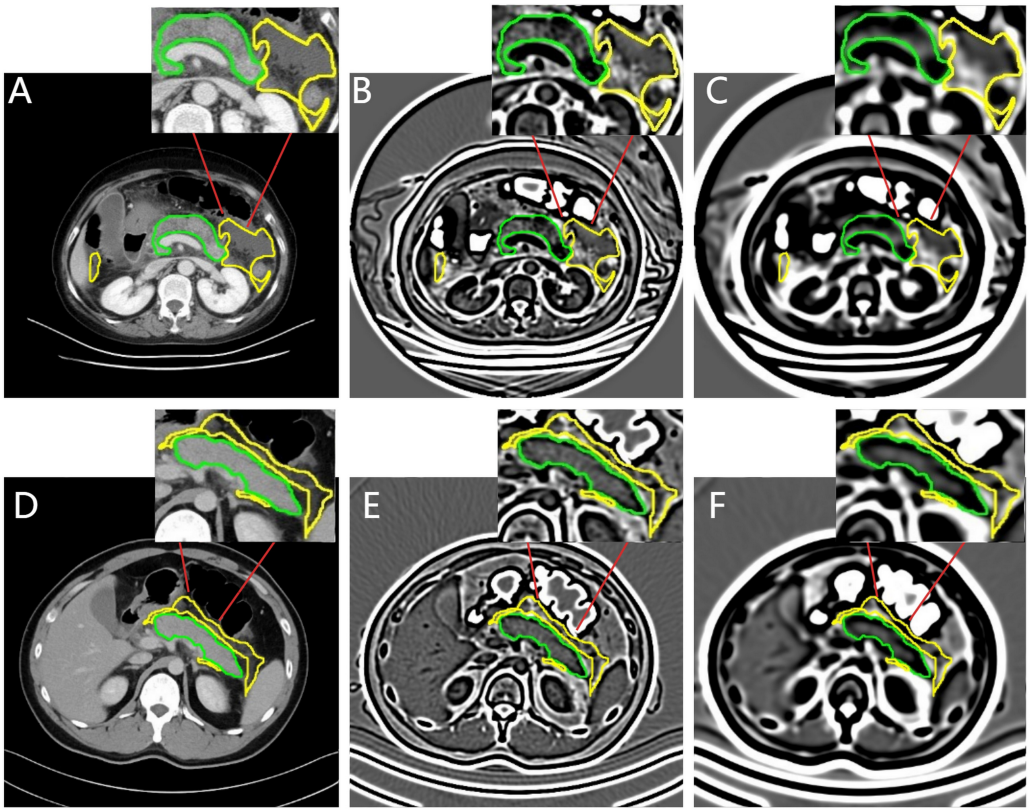

Fig. 2. Laplacian of Gaussian (LoG) filtered images. (A) Severe acute pancreatitis (SAP) original image. (B) SAP LoG filtered image ($\sigma = 2$). (C) SAP LoG filtered image ($\sigma = 4$). (D) Non-severe acute pancreatitis (NSAP) original image. (E) NSAP LoG filtered image ($\sigma = 2$). (F) NSAP LoG filtered image ($\sigma = 4$).

higher values are observed for this feature. Visually, the peripancreatic ROI in Fig. 2E appears more disorganized compared to the grey-scale texture in Fig. 2B, indicating greater heterogeneity in the exudate region.

Logarithmic Filter

The logarithmic filter formula and logarithmic function curves are detailed in Table 1. Observing the nature of the logarithmic function, it is evident from the logarithmic function image that the function exhibits a steeper slope in lower grey level areas, gradually tapering off in higher grey level areas. In the corresponding image, this implies that the low grey level interval in the image can be expanded, whereas the high grey level interval is compressed. Following logarithmic filtering, the contrast between the low grey level areas of the image and the background tissue is heightened. This enhancement facilitates a clearer display of details in the low grey level areas [10].

In Table 3, features 2 and 5 were identified as representative features after logarithmic filtering. Feature 2 signifies that after logarithmic filtering of the image, the GLSZM was computed, and subsequently, the "LowGrayLevelZoneEmphasis" value was derived. A larger "LowGrayLevelZoneEmphasis" indicates a higher occurrence of connected areas with low grey levels. As depicted in panels B and D of Fig. 3, logarithmic-filtered images of one case of SAP and one case of NSAP are shown, respectively. In this dataset, the mean value for NSAP was 0.00759, while for SAP, it was 0.00457, and this difference was statistically significant ($p < 0.001$). This implies that SAP tends to exhibit a lower value for this feature, suggesting that SAP had fewer connected areas with low grey levels in the ROI compared to NSAP.

Feature 5 indicates that after logarithmic filtering of the image, the GLCM was computed, and subsequently, the "DifferenceAverage" value was calculated. The rows and columns of the GLCM represent different grey levels, and the matrix elements count the number of times a particular grey pair occurs. The "DifferenceAverage" calculates the average difference in grey scale pairs in the peripancreatic region, with larger values indicating greater differences in grey scale between adjacent pixels.

In this dataset, the mean value for NSAP was 9.51, while for SAP, it was 17.8, and this difference was statistically significant ($p < 0.001$). This suggests that the adjacent pixel greyscale difference was greater in the SAP images. As shown in Fig. 3B,D comparatively, the variation in adjacent grey scale is more pronounced in Fig. 3B.

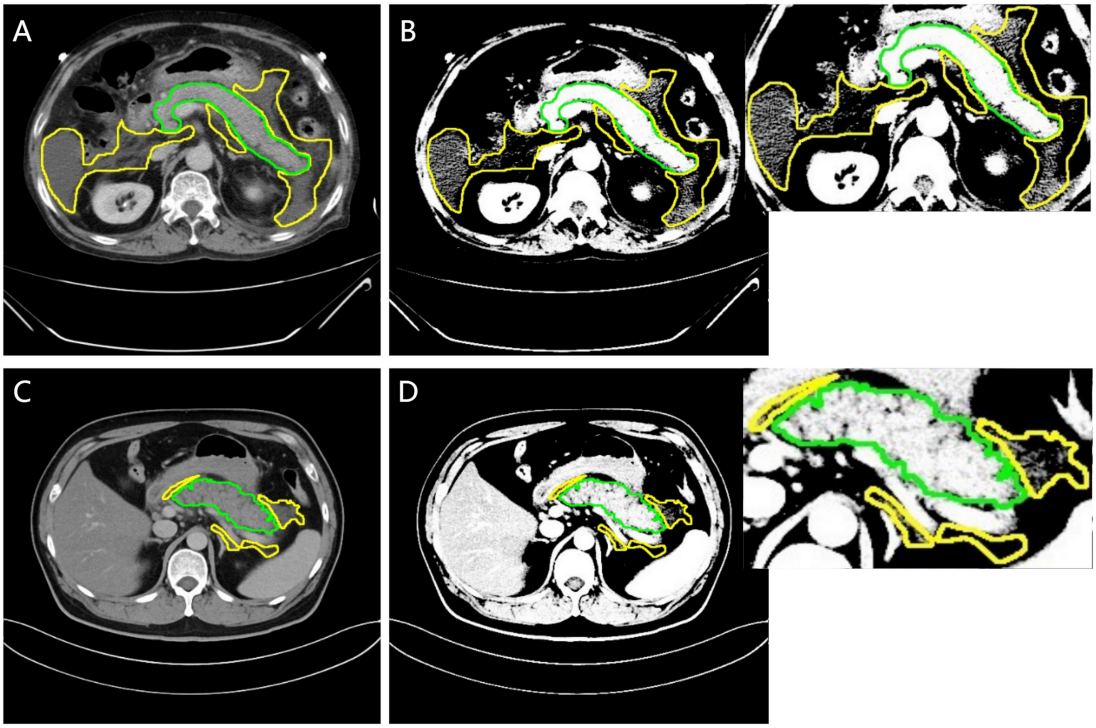

Fig. 3. Log filtered images. (A) SAP original image. (B) SAP log filtered image. (C) NSAP original image. (D) NSAP log filtered image.

Gradient Filter

The gradient filter formula and the one-dimensional center filter template are presented in Table 1.

This filter template is utilized to obtain the gradient image by subtracting the grey-scale values of adjacent center pixels. The resulting gradient filters enhance the outlines of each tissue and organ structure. In the gradient image, contours and texture edges of organ structures are displayed differently—texture edges are tightly distributed, while contours change more rapidly relative to their surrounding grey levels and are typically isolated edges of greater greyscale intensity [11].

The ROI grey scale varies depending on the severity of the pathological changes occurring in the pancreas and peri-pancreas during AP, such as peri-pancreatic fluid, pancreatic edema, pancreatic or peri-pancreatic necrosis, etc. Consequently, the ROI is segmented by varying degrees of linear margins in the gradient-filtered images. As peripancreatic exudate or effusion increases, the change in pancreatic parenchyma and peripancreatic fat grey scale diminishes or disappears, leading to discontinuities in pancreatic margins or the inability to identify pancreatic morphology (Fig. 4).

In Table 3, features 3 and 6 were identified as representative features after gradient filtering. Feature 3 signifies that after the gradient filtering of the image, the GLCM was calculated, and subsequently, the "JointEntropy" value was computed. A larger "glcm_JointEntropy" indicates a higher occurrence of adjacent repetitive grey pairs, and the image tends to exhibit a more homogeneous fine texture. As illustrated in panels C and D of Fig. 4, gradient-filtered images of one case of NSAP and one case of SAP are shown, respectively. In this dataset, the mean value for NSAP was 0.464, whereas for SAP, it was 0.233, and this difference was statistically significant ($p < 0.001$). This suggests that SAP tends to exhibit a lower value for this feature, indicating that SAP images have fewer occurrences of adjacent repeated grey pairs, and the fine-texture style of the image tends to be different.

Feature 6 suggests that after the gradient filtering of the image, the GLDM was calculated, and subsequently, the "DependenceVariance" value was computed. A smaller value of "gldm_DependenceVariance" implies a more consistent size of the same grey area within the δ range.

In this dataset, the mean value for NSAP was 26.7, which was lower than the mean value of 36.9 for SAP. This difference indicates that the fine texture style of SAP tends to be different, as observed from the gradient images.

Exponential and Square Filters

The exponential and logarithmic functions are inverse functions of each other. As illustrated in Table 1, based on the function curve, the exponential function stretches the grey interval in high grey level areas, while compressing the grey interval in low grey level areas.

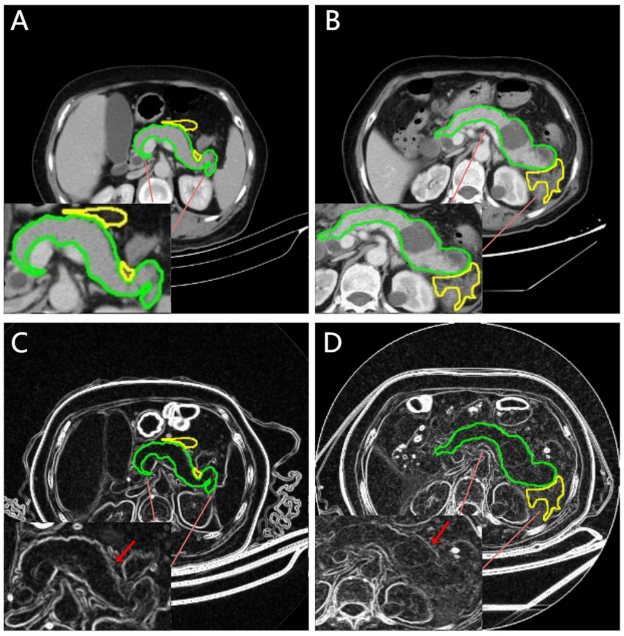

Fig. 4. Gradient filtered images. (A) NSAP original image. (B) SAP original image. (C) NSAP gradient filtered image, where the morphology of the pancreas can be identified. (D) SAP gradient filtered image, where the margins of the pancreas are discontinuous and the morphology of the pancreas is poorly defined, with a circular border being seen in the body of the pancreas and the tail of the pancreas also divided by the linear.

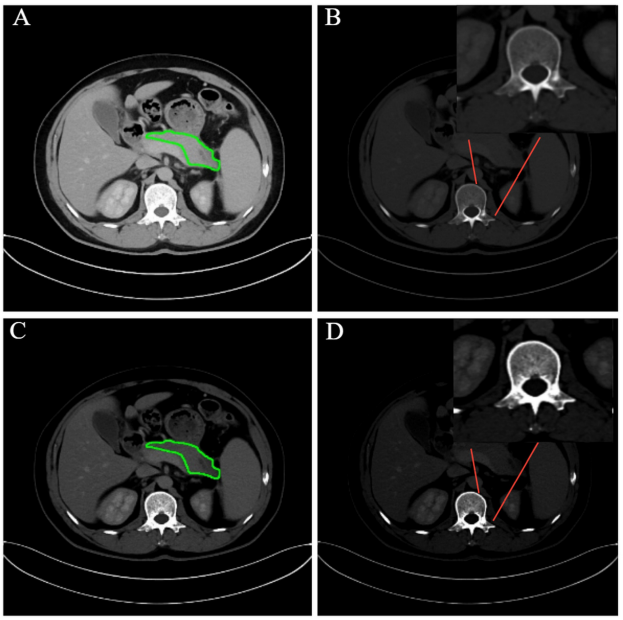

Fig. 5. Exponential filtered images. (A) Original abdominal window image. (B) Original bone window image. (C,D) Exponential filtered images, (C) suitable for viewing the pancreatic region, and (D) suitable for viewing the bone.

In the case of the square filter, due to the square operation, negative CT values are flipped to positive values. Similar to the exponential filter, this filter widens the high absolute values of the grey interval while compressing the low absolute values of the grey interval.

In this study, the acquired images primarily focused on pancreatitis, with emphasis on the pancreas and peripancreatic regions. The CT values within the associated ROI were predominantly concentrated in the low and medium grey level areas. Consequently, applying the exponential and square filters resulted in a compression of the grey interval in the target area, offering limited additional visual indicators compared to the original image.

However, it's worth noting that there was still value in exploring the high grey level areas for study. This is exemplified in Fig. 5, where the exponentially filtered image provides better detail of the thoracic spine compared to the original bone window. This underscores the potential utility of these filters in highlighting specific features or structures that may not be as prominent in the original image.

Discussion

This study primarily introduced and applied LoG, logarithmic, exponential, square, and gradient filters in radiomics. The focus was on exploring the complementary features of AP portal venous phase CT images post-filtering. The LoG Filter and Gradient Filter were employed to strengthen edges or region boundaries with significant changes in image greyscale, particularly effective in emphasizing areas with pronounced variations in image intensity. Logarithmic filtering was mainly used to extend the low grey levels of the image, facilitating the display of details in low grey areas and enhancing visibility and contrast in regions with lower intensity. In contrast, the exponential filter stretched the high grey levels of the image, suitable for viewing details in high grey areas and bringing out features that may be less pronounced in the original image. The square filter was employed to enhance the contrast between pixels with high grey levels and similar grey levels, particularly useful for displaying details in high grey level areas and areas with similar grey levels. Each filter served a specific purpose in modifying the image characteristics, allowing for a more nuanced exploration of features in different intensity ranges.

In LoG images, the pancreatic region of SAP displayed fewer small areas of repetitive greyscale within the δ range. The peripancreatic region of SAP exhibited higher uncertainty and more irregularity in both area size and the distribution of grey levels in grey-scale repetition. In the pancreatic region of logarithmic images, SAP showed less connection in low-gray-scale. In the peripancreatic region, SAP demonstrated a larger average variance in the grayscale of two neighboring pixels. In gradient images, SAP demonstrated less repetition of two adjacent pixel greyscales in the pancreatic region, with more inhomoge-

neous fine textures. SAP exhibited irregularities in the size of the same greyscale region within the δ range of the peripancreatic region.

All three filtered images depicted the same structure from different perspectives, indicating that the pancreatic region of SAP had a coarser textural structure, while the peripancreatic region of SAP exhibited greater pixel variation in small areas, higher grey-scale uncertainty, and more disorganized subtleties. This observation was consistent with the pathological interpretation of acute pancreatitis.

In pathology, AP is generally divided into interstitial edematous pancreatitis (IEP) and necrotizing pancreatitis (NP) [12]. In the former, there is limited or diffuse edema of the pancreas with surface congestion, thickened lobular septa, few scattered foci of hemorrhagic necrosis, infrequent significant vascular changes, and less clear exudate. In the latter case, the main changes of the pancreas are extensive hemorrhagic necrosis of the pancreatic tissue, blurring of the lobular structures on the pancreatic surface, cloudy fluid in the abdominal cavity, and often peripancreatic fatty tissue necrosis.

In medical practice, effective extraction of image edge information with medical images is crucial for disease diagnosis [13–15]. Both LoG and gradient filters in radiomics prove sensitive to edges exhibiting significant changes in image greyscale. The gradient filter, being a first-order differential operator, typically yields broader edges. However, due to the absence of image smoothing, it results in increased image noise, somewhat impacting image quality and potentially interfering with visual observation.

The LoG operator is one of the second-order differential operators. Unlike the gradient filter, it is isotropic and capable of meeting the requirements for edge sharpening for various orientations. Simultaneously, LoG demonstrated heightened sensitivity to detailed information. It can analyze textures ranging from fine to coarse and mitigate photon noise in CT images, thereby enhancing the ability to quantify disease heterogeneity [16].

Radiomics image preprocessing filters were applied to the entire image rather than being confined to separate ROIs, and the outcomes varied across different ROIs despite using the same filter. In their study, Chen *et al*. [17] selected two sets of optimal radiomics features, both of which comprised exponential-based features while excluding logarithmic-based features. This choice might be attributed to the concentration of pixel values in high grey-level areas within chest CT images of lung adenocarcinoma lesions. The exponential filter serves to stretch the interval between the high grey levels of the image, making it suitable for observing details in areas with high grey levels. Consequently, if the ROI exhibits high grey levels in the original image, the exponential filter effectively highlights its details. Conversely, the logarithmic filter stretches the interval between the lower grey levels of the image, facilitating the presentation of details in lower grey areas. Therefore, if the ROI possesses low grey levels in the original image, its details become more evident when logarithmically filtered.

The squared filter enhances the dissimilarity between pixels with similar grey levels by squaring the original intensities, thereby boosting contrast. However, it also has the effect of eliminating contrast between tissues with the same original grey level but differing in positive and negative polarity.

Nevertheless, this study had some limitations: (1) Not all image types were included in the presentation, and we intend to investigate the image features of the remaining filtered images in the subsequent phase. (2) Only the portal venous phase AP image features were examined. Therefore, we plan to extend our observations to encompass filtering features related to different diseases, considering various time phases and disease conditions.

Conclusions

Various filters exhibit distinct image features. The selection of appropriate filter maps for feature extraction is guided by the characteristics of the ROI to comprehensively capture the heterogeneity of the disease. Our study introduces a potentially innovative approach or research idea for clinical review.

Availability of Data and Materials

The datasets generated during and/or analyzed during the current study are available from the corresponding author upon reasonable request.

Author Contributions

WJH, MYT, XJ, BX and XWC designed the research study; All authors performed the research; XJ, YMZ, JYW and YZZ collected and analyzed the data. WJH and XJ have been involved in drafting the manuscript and all authors have been involved in revising it critically for important intellectual content. All authors give final approval of the version to be published. All authors have participated sufficiently in the work to take public responsibility for appropriate portions of the content and agreed to be accountable for all aspects of the work in ensuring that questions related to its accuracy or integrity.

Ethics Approval and Consent to Participate

This retrospective study received approval from the ethics committee of North Sichuan Medical College (No. NSMC lunzhiwenshen[2023030]), and patients were exempted from providing informed consent.

Acknowledgment

Not applicable.

Funding

This work was partly supported by the Project of Sichuan Natural Science Foundation (No. 2023NSFSC0646), and was also partly supported by the Bureau of Science & Technology Nanchong City (No. 20SXQT0315).

Conflict of Interest

The authors declare no conflict of interest.

References

[1] Boxhoorn L, Voermans RP, Bouwense SA, Bruno MJ, Verdonk RC, Boermeester MA, *et al*. Acute pancreatitis. Lancet. 2020; 396: 726–734.

[2] Zhao Y, Wei J, Xiao B, Wang L, Jiang X, Zhu Y, *et al*. Early prediction of acute pancreatitis severity based on changes in pancreatic and peripancreatic computed tomography radiomics nomogram. Quantitative Imaging in Medicine and Surgery. 2023; 13: 1927–1936.

[3] Li M, Fu S, Zhu Y, Liu Z, Chen S, Lu L, *et al*. Computed tomography texture analysis to facilitate therapeutic decision making in hepatocellular carcinoma. Oncotarget. 2016; 7: 13248–13259.

[4] Ganeshan B, Miles KA. Quantifying tumour heterogeneity with CT. Cancer Imaging. 2013; 13: 140–149.

[5] Yasaka K, Akai H, Mackin D, Court L, Moros E, Ohtomo K, *et al*. Precision of quantitative computed tomography texture analysis using image filtering: A phantom study for scanner variability. Medicine. 2017; 96: e6993.

[6] Banks PA, Bollen TL, Dervenis C, Gooszen HG, Johnson CD, Sarr MG, *et al*. Classification of acute pancreatitis–2012: revision of the Atlanta classification and definitions by international consensus. Gut. 2013; 62: 102–111.

[7] Mayerhoefer ME, Materka A, Langs G, Häggström I, Szczypiński P, Gibbs P, *et al*. Introduction to Radiomics. Journal of Nuclear Medicine. 2020; 61: 488–495.

[8] Zwanenburg A, Leger S, Vallières M, Löck S. Image biomarker standardisation initiative - feature definitions. 2017. Available at: https://arxiv.org/abs/1612.07003v3. (Accessed: 14 March 2022).

[9] Chen S, Yao L, Chen B. A parameterized logarithmic image processing method with Laplacian of Gaussian filtering for lung nodule enhancement in chest radiographs. Medical & Biological Engineering & Computing. 2016; 54: 1793–1806.

[10] Singh N, Bhandari AK. Image contrast enhancement with brightness preservation using an optimal gamma and logarithmic approach. IET Image Process. 2020; 14: 794–805.

[11] Qu ZG, Wang P, Gao YH, Wang P, Shen ZK. Frequency domain filtering of gradient image for contour detection. Optik. 2013; 124: 1398–1401.

[12] Gerosa M, Chiarelli M, Maggioni D, Cioffi U, Guttadauro A. Acute biliary pancreatitis: the current role of endoscopic and minimally invasive surgical procedures. Annali Italiani di Chirurgia. 2023; 94: 36–44.

[13] Li X, Wee WG. Retinal vessel detection and measurement for computer-aided medical diagnosis. Journal of Digital Imaging. 2014; 27: 120–132.

[14] Bayraktar M, Kockara S, Halic T, Mete M, Wong HK, Iqbal K. Local edge-enhanced active contour for accurate skin lesion border detection. BMC Bioinformatics. 2019; 20: 91.

[15] Moldovanu S, Moraru L, Biswas A. Edge-based structural similarity analysis in brain MR images. Journal of Medical Imaging and Health Informatics. 2016; 6: 539–546.

[16] Shen Q, Shan Y, Hu Z, Chen W, Yang B, Han J, *et al*. Quantitative parameters of CT texture analysis as potential markers-for early prediction of spontaneous intracranial hemorrhage enlargement. European Radiology. 2018; 28: 4389–4396.

[17] Chen Q, Li Y, Cheng Q, Van Valkenburgh J, Sun X, Zheng C, *et al*. EGFR Mutation Status and Subtypes Predicted by CT-Based 3D Radiomic Features in Lung Adenocarcinoma. OncoTargets and Therapy. 2022; 15: 597–608.